Hierarchical γ-Al_2O_3 monoliths with highly ordered 2D hexagonal mesopores in macroporous walls†

Le-Le Li, Wen-Tao Duan, Quan Yuan, Zhen-Xing Li, Hao-Hong Duan and Chun-Hua Yan*

Received (in Cambridge, UK) 25th June 2009, Accepted 22nd August 2009
First published as an Advance Article on the web 10th September 2009
DOI: 10.1039/b912495k

Hierarchical γ-Al_2O_3 monoliths with interconnected macroporous architecture and highly ordered 2D hexagonal mesostructure have been synthesized by using nonionic triblock copolymer and polyurethane foam as co-templates.

Since the discovery of ordered mesoporous silica,[1] due to the wide application of alumina as adsorbents, catalysts and catalyst supports, great efforts have been devoted to the synthesis of mesoporous alumina.[2–10] Unfortunately disordered structures with amorphous walls were fabricated in most cases.[2] Recently, ordered mesoporous aluminas have been synthesized by a modified sol–gel route in the presence of block copolymers,[3,4] aerosol-assisted self-assembly with use of block copolymers,[5,6] nanocasting process with mesoporous carbon (CMK-3) as hard template,[7] and evaporation-induced self-assembly (EISA).[8,9] Furthermore, the potential applications of mesoporous alumina can only be maximized in the highly crystalline state.[4–10] However, all syntheses of mesoporous alumina reported so far only lead to the fabrication of powders or films,[2–10] and not of monolithic materials, which refers to uniform structures composed of interconnected macrocells. In particular, monolithic materials with hierarchically multiscale porosity is an extensive field of investigation. Such materials not only enable high surface areas and high chemical activity sites (associated with micro- or mesoporous structure), but also allow for processing bulky molecules/species efficiently with fast diffusion to and from the active sites within the mesopores (associated with macroporous structure).[11] These features are of great interest for a wide range of applications such as separation and as supports for flow-through systems, *e.g.*, catalysts and sensing.[12] Until now only a few reports have been available where mesoporous metal oxide monoliths other than silica-based monoliths were prepared.[12] To our knowledge, there has been no report on macroporous γ-Al_2O_3 monoliths with ordered mesopores on the walls.

Here we describe the synthesis of bimodal macroporous γ-Al_2O_3 monoliths with highly ordered crystalline mesoporous walls. The general synthesis strategy is based on a simple sol–gel process by using a conventional polyurethane (PU) foam replication method combined with a triblock copolymer P123 as mesoporous structure-directing agents. The synthetic mechanism of the hierarchically porous aluminas can be described as follows (also see ESI†, Fig. S1). The primary sol is prepared with aluminium isopropoxide as the inorganic precursor, nitric acid as the acid adjustor, and P123 as the surfactant, and all of which dissolved in ethanol as a transparent solution. When the PU foam is impregnated into the sol solution, the sol enters into the interconnected macropore voids by capillary and wetting driving forces. Then during the solvent evaporation, cross-linked aluminium species can assemble with the triblock copolymer P123 to form the ordered mesophases on the interior surface of the PU struts, resulting in a solvent-evaporation-induced coating and self-assembly process.[13] The factors governing this self-assembled formation of ordered mesostructures were studied. It was found that the temperature played an important role. After finely tuning this factor, 40 °C is found to be the optimized condition and was adopted in the present work. After final appropriate calcination, the PU sponge and P123 can be removed, and an effective replica of the PU sponge with mesoporous structured alumina monolith is obtained.

As shown in the photographs of our typical samples (Fig. 1(a)), the as-made alumina materials retain the original uniform morphologies of the used PU foam with different shrinkages due to calcinations at various temperatures. A typical alumina monolith calcined at 550 °C is large in size, with a length of 2.0 cm, width of 1.9 cm and height of 0.6 cm. Its shrinkage is calculated to be about 28% in linear dimensions. The size of the monoliths can be easily adjusted, since the used PU foam with different geometries can be prepared simply by cutting it into the desired shapes and sizes. Representative scanning electron microscopy (SEM) images of the alumina monoliths calcined at different temperatures are shown in Fig. 1(b) and (c). Fig. 1(b) shows that the alumina materials calcined at 550 °C exhibit a macroporous structure with interconnected open pores of 400–600 μm in size and thickness of the pore walls of about 50 μm. After calcination at 900 °C, the samples retain a 3D uniform macrostructure with the size of the interconnected macropores reduced slightly (Fig. 1(c)) due to the shrinkage during the calcination process at higher temperature, which is in agreement with the observed slight decrease of size of the materials. It is reasonable to deduce that macropore size of the materials could be tuned by using commercially available PU foam with different pore diameters as replica templates.

Fig. 2(a) shows the small-angle X-ray diffraction (XRD) patterns of the as-synthesized alumina materials. The sample calcined at 550 °C shows a very sharp diffraction peak around 1.2° and one weak peak around 2.1°, which can be attributed

Beijng National Laboratory for Molecular Science, State Key Laboratory of Rare Earth Materials Chemistry and Applications, PKU-HKU Joint Laboratory on Rare Earth Materials and Bioinorganic Chemistry, Peking University, 100871, Beijing, China. E-mail: yan@pku.edu.cn; Fax: +86 10 6275 4179; Tel: +86 10 6275 4179

† Electronic supplementary information (ESI) available: Detailed synthesis procedures and additional experimental results. See DOI: 10.1039/b912495k

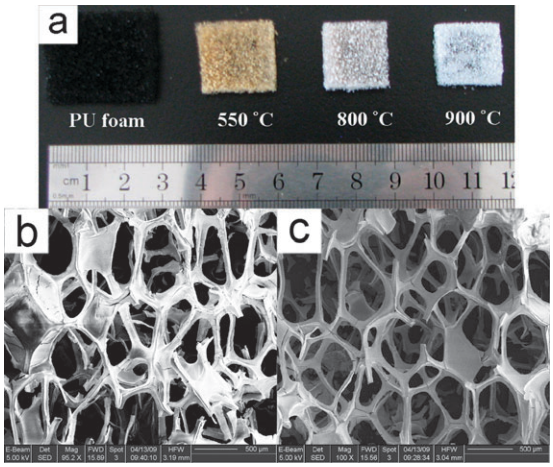

Fig. 1 (a) Representative photographs of the used polyurethane (PU) foam and the as-made alumina monoliths after calcination at various temperatures. SEM images of the as-made alumina monoliths calcined at 550 °C (b) and 900 °C (c), respectively.

to a 2D hexagonal (*P6mm*) cell, as confirmed by the transmission electron microscopy (TEM) images (see below). The well-expressed reflections show that a good mesoscopic order is retained even after calcination at 800 and 900 °C, indicating a high thermal stability of the mesoporous structure. Fig. 2(b) shows the wide-angle XRD patterns of the alumina samples calcined at different temperatures. Calcination at 550 °C gives rise to a mesostructure with amorphous walls. Moreover, the amorphous framework walls were transformed into γ-Al_2O_3 phase (JCPDS No. 10-0425) after further treatment at a temperature of 800 °C. The combination of the small- and wide-angle XRD data convinces us that highly ordered mesoporous γ-Al_2O_3 with crystalline walls can be prepared. In general, high crystallinity and controlled mesoporosity are highly desirable for many applications.

Fig. 3(a) and (b) show the TEM images of the samples calcined at 550 °C. The 2D hexagonal mesostructure is further confirmed, as a highly ordered hexagonal array of mesopores with 1D cylindrical channels viewed along the [001] and [110] directions, respectively, is clearly observed. The lattice parameter (9.0–9.6 nm) observed by TEM corresponds well with that calculated from the d_{100} spacing in the XRD pattern. The TEM images (Fig. 3(c) and (d)) also verify that

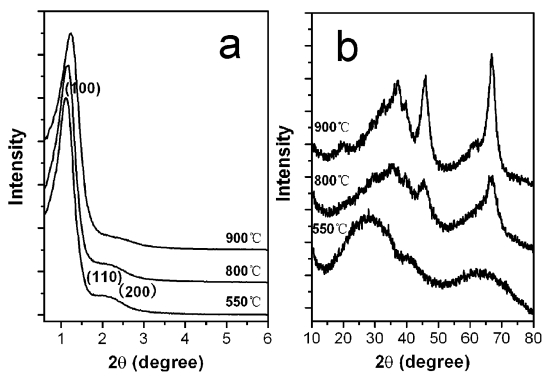

Fig. 2 (a) Small- and (b) wide-angle XRD patterns of the alumina monoliths calcined at different temperatures.

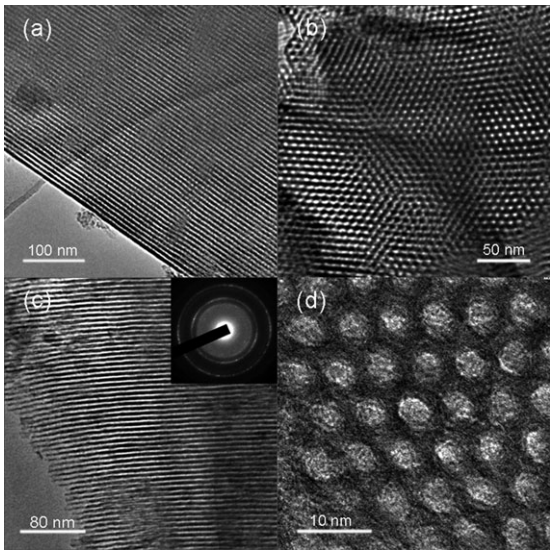

Fig. 3 TEM images of the hierarchical alumina monolith calcined at 550 °C viewed along (a) [110] and (b) [001] directions. TEM images of an alumina monolith calcined at 900 °C viewed along (c) [110] and (d) [001] directions (the inset in (c) is the corresponding SAED pattern).

the ordered mesoporous structures are retained even after 900 °C treatment. The selective area electron diffraction (SAED) pattern (inset in Fig. 3(c)) of the ordered mesostructure domains confirms that the mesoporous wall is crystalline with γ-Al_2O_3 phase. Additional proof for the crystallinity of the frameworks is given by high-resolution TEM investigation (ESI,† Fig. S2), which reveals the existence of several nanocrystallites with well-defined lattice planes.

The alumina monoliths retain sharply distributed mesopores on the macroporous walls as further evidenced by nitrogen adsorption–desorption measurements. Fig. 4 shows nitrogen adsorption–desorption isotherms and corresponding pore size distribution of the alumina samples treated at different temperatures. In all cases, the isotherms can be ascribed to type IV with H1-shaped hysteresis loops, suggesting their uniform cylindrical pores. The sample treated at 550 °C has a large BET surface area of 300 $m^2\ g^{-1}$ and a pore volume of 0.40 $cm^3\ g^{-1}$. When transformed into γ-alumina, it still exhibits a BET surface area of 209 and 178 $m^2\ g^{-1}$ at 800 and 900 °C, respectively. Barrett–Joyner–Halenda calculations for the pore-size distribution, derived from desorption data, reveal a narrow distribution centered at 2.9–3.4 nm, which coincides well with the small-angle XRD and TEM results. The large surface areas and hierarchically porous structure combined with excellent thermal stability enhance the potential applications of these γ-Al_2O_3 monoliths in catalysis.

Since alumina is a highly effective support in catalysis, the successful preparation of mesoporous alumina monolith stimulated us to extend this approach to the one-pot synthesis of hierarchical alumina-supported metal oxide monoliths. To illustrate the feasibility of this strategy we present here the synthesis of alumina-supported nickel aluminate because of its importance in catalysis.[14] As is known, the direct preparation of mesoporous multimetallic oxides is still a challenge because it should meet two crucial requirements, *i.e.*, (1) to homogenously distribute each component in the precursor solution

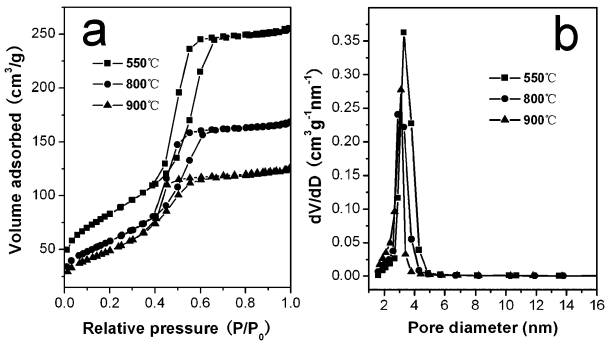

Fig. 4 (a) Nitrogen adsorption–desorption isotherms and (b) pore-size distributions of the mesoporous alumina monoliths calcined at various temperatures.

and (2) to avoid macroscopic phase separation during the self-assembly process.[6] Fortunately, our method can satisfy these requirements. Both small-angle XRD measurement (Fig. 5(a)) and TEM images (ESI,† Fig. S3) reveal that the ordered mesostructure of the Ni-containing monolith is still preserved even after the addition of 12 mol% of the aforementioned metal. Wide angle XRD patterns (Fig. 5(b)) for these samples show that calcination at 550 °C gives rise to the mesostructure with amorphous walls, and then nickel aluminate ($NiAl_2O_4$) spinel phase (JCPDS No. 10-0339) appears after further treatment at 900 °C. The absence of individual NiO phases support the evidence that the latter phases were homogeneously mixed.[14a] Photographs (inset of Fig. 5(a)) and SEM observation (ESI†, Fig. S4) of the $NiAl_2O_4$ monolith show a blue uniform appearance composed of interconnected open pores of 300–600 μm. Nitrogen adsorption–desorption analysis (ESI,† Fig. S5) show a narrow pore-size distribution of 3–6 nm and BET surface area of 241 and 190 $m^2\ g^{-1}$ for the samples calcined at 550 and 900 °C, respectively. These mesoporous monolithic $NiAl_2O_4$ spinels can be applied to catalytic fields,[14] where high surface area, controlled porosity with a high loading of catalytically active metal oxides, excellent mass transport, and good nanocrystallinity are simultaneously required.

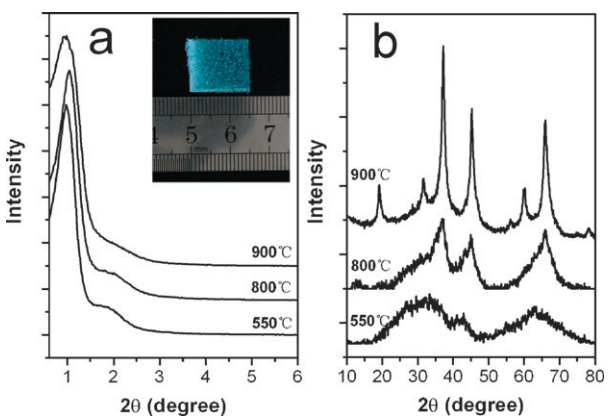

Fig. 5 (a) Small- and (b) wide-angle XRD patterns of the Ni-containing alumina monoliths calcined at different temperatures. The inset shows a representative photograph of the alumina-supported $NiAl_2O_4$ monolith calcined at 900 °C.

In summary, we have developed a facile and highly efficient synthetic strategy for the fabrication of macroporous alumina monoliths with highly ordered amorphous and/or crystalline γ-alumina mesoporous walls. The hierarchical materials exhibit fully interconnected macropores of 400–600 μm in size and uniform mesopores of 2.9–3.4 nm; the materials exhibit high surface areas and high thermal stability. Furthermore, the process can be successfully applied to the synthesis of alumina-based multicomponent mesoporous monoliths with high framework crystallinity. We believe that the simplicity, versatility and reproducibility of this approach will facilitate the large-scale industrial production of new mesoporous monolithic materials. Future studies will be devoted to the exploration of catalytic applications of these hierarchical single- and multi-component mesoporous alumina monoliths.

This work was supported by NSFC (20671005 and 20821091), NSFC-RGC (20731160001), MOST of China (2006CB601104).

Notes and references

1 C. T. Kresge, M. E. Leonowicz, W. J. Roth, J. C. Vartuli and J. S. Beck, *Nature*, 1992, **359**, 710; D. Zhao, J. Feng, Q. Huo, N. Melosh, G. H. Fredrickson, B. F. Chmelka and G. D. Stucky, *Science*, 1998, **279**, 548.
2 S. A. Bagshaw, E. Prouzet and T. J. Pinnavaia, *Science*, 1995, **269**, 1242; F. Vaudry, S. Khodabandeh and M. E. Davis, *Chem. Mater.*, 1996, **8**, 1451; M. Yada, M. Ohya, M. Machida and T. Kijima, *Chem. Commun.*, 1998, 1941; S. Cabrera, J. E. Haskouri, J. Alamo, A. Beltrán, D. Betrán, S. Mendioroz, M. D. Marcos and P. Amorós, *Adv. Mater.*, 1999, **11**, 379; S. A. Bagshaw and T. J. Pinnavaia, *Angew. Chem., Int. Ed. Engl.*, 1996, **35**, 1102; W. Zhang and T. J. Pinnavaia, *Chem. Commun.*, 1998, 1185.
3 K. Niesz, P. Yang and G. A. Somorjai, *Chem. Commun.*, 2005, 1986.
4 Z. R. Zhang, R. W. Hicks, T. R. Pauly and T. J. Pinnavaia, *J. Am. Chem. Soc.*, 2002, **124**, 1592; Z. R. Zhang and T. J. Pinnavaia, *J. Am. Chem. Soc.*, 2002, **124**, 12294.
5 C. Boissière, L. Nicole, C. Gervais, F. Babonneau, M. Antonietti, H. Amenitsch, C. Sanchez and D. Grosso, *Chem. Mater.*, 2006, **18**, 5238.
6 C.-K. Tsung, J. Fan, N. Zheng, Q. Shi, A. J. Forman, J. F. Wang and G. D. Stucky, *Angew. Chem., Int. Ed.*, 2008, **47**, 8682.
7 Q. Liu, A. Q. Wang, X. D. Wang and T. Zhang, *Chem. Mater.*, 2006, **18**, 5153.
8 M. Kuemmel, D. Grosso, C. Boissière, B. Smarsly, T. Brezesinski, P. A. Albouy, H. Amenitsch and C. Sanchez, *Angew. Chem., Int. Ed.*, 2005, **44**, 4589.
9 P. D. Yang, D. Y. Zhao, D. I. Margolese, B. F. Chmelka and G. D. Stucky, *Nature*, 1998, **396**, 152; Q. Yuan, A. X. Yin, C. Luo, L. D. Sun, Y. W. Zhang, W. T. Duan, H. C. Liu and C. H. Yan, *J. Am. Chem. Soc.*, 2008, **130**, 3465.
10 Z. R. Zhang and T. J. Pinnavaia, *Angew. Chem., Int. Ed.*, 2008, **47**, 7501.
11 A. El Kadib, R. Chimenton, A. Sachse, F. Fajula, A. Galarneau and B. Coq, *Angew. Chem., Int. Ed.*, 2009, **48**, 4969; M.-O. Coppens, J. Sun and T. Maschmeyer, *Catal. Today*, 2001, **69**, 331.
12 A.-H. Lu and F. Schüth, *Adv. Mater.*, 2006, **18**, 1793; J.-H. Smått, B. Spliethoff, J. B. Rosenholmb and M. Lindén, *Chem. Commun.*, 2004, 2188; J.-H. Smått, C. Weidenthaler, J. B. Rosenholmb and M. Lindén, *Chem. Mater.*, 2006, **18**, 1443.
13 C. J. Brinker, Y. F. Lu, A. Sellinger and H. Y. Fan, *Adv. Mater.*, 1999, **11**, 579; X. Li, X. Wang, H. Chen, P. Jiang, X. Dong and J. Shi, *Chem. Mater.*, 2007, **19**, 4322; C. Xue, B. Tu and D. Zhao, *Adv. Funct. Mater.*, 2008, **18**, 1.
14 S. M. Morris, P. F. Fulvio and M. Jaroniec, *J. Am. Chem. Soc.*, 2008, **130**, 15210; F. Negrier, E. Marceau and M. Che, *Chem. Commun.*, 2002, 1194; E. Heracleous, A. F. Lee, K. Wilson and A. A. Lemonidou, *J. Catal.*, 2005, **231**, 159.

